# Mathematical modeling of traveling-wave electroosmotic micropumps by using of the Weak Form

J. Hrdlicka[1], P. Cervenka[1] and D. Snita[1]
[1]Institute of Chemical Technology Prague, Department of Chemical Engineering
*Corresponding author: Jiri.Hrdlicka@seznam.cz

**Abstract:** Mathematical model of the AC electro-osmotic micropump based on the Poison-Nernst-Planck equation, the Navier-Stokes equation and the equation of continuity has been extended by description of the microfluidic channel surroundings. This contribution is dedicated to the analysis of the preliminary results obtained from the innovated model with a new digital (discontinuous) driving mode.

**Keywords:** ac electro-osmosis, microfluidics

## 1. Introduction

The AC electro-osmotic micropumps seem to be a promising alternative to classical pumps at micro- and nano-scale, due to the absence of moving parts. These pumps consist of the powered arrays of coplanar metallic electrodes placed on a microchannel wall(s) [1]. Proper choice of electrode array geometry or driving signal can produce a stable net flow accompanied with a slight pulsation around the average flow velocity [2].

The electroosmotic micropumps generate an electroosmotic flow of electrolytes. Charged electrodes cause the electrolyte polarization, which results in the formation of clouds of ions, the electric double layers, above the electrodes. Component of the electric field, which is tangential to the channel walls, than accelerates the ions along the surface and the electrolyte bulk is dragged by viscous forces.

We examined traveling-wave electroosmotic pumps [3], which are usually powered by a sinusoidal AC signal. The discontinuous driving and an implementation of microchannel surroundings require use of the weak form due to its capability to describe more general class of boundary conditions and handle model singularities.

## 2. Mathematical description

The electroosmotic pump arrays have a periodical character. Symmetries involved in model and geometry allow reducing modeling domain to a periodic segment of the ac electroosmotic micropump. Chain of such segments forms the pump itself. The computational domain $D$ can be subdivided according to the material into the electrolyte, metal and dielectric parts. The model electrolyte is assumed to be a symmetric, uni-univalent, Newtonian, incompressible fluid. Metallic electrodes are supposed to be made from Copper or Gold. Dielectric materials are supposed to be made of glass or poly-dimethyl-siloxane.

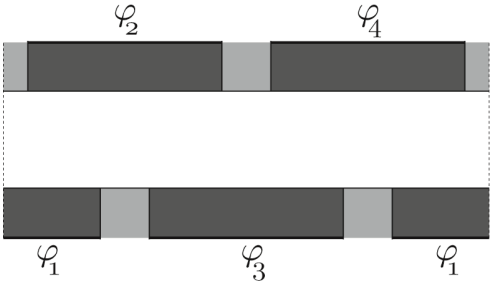


**Figure 1**. A single periodical segment of the ac electro-osmotic pump. The dark grey boxes and the light grey boxes represent the electrodes and the dielectric walls, respectively. Solid lines denote the phase interfaces. The thick lines represent source sides of the electrodes with the temporarily fixed electric potential. The dashed lines denote the periodically coupled borders.

Following dependent variables are used to describe the pump behavior

$$\varphi(\mathbf{x},t), c(\mathbf{x},t), q(\mathbf{x},t), \mathbf{v}(\mathbf{x},t), p(\mathbf{x},t)$$

represent the electric potential, the electrolyte average salt concentration, the electric charge density, the velocity vector and the pressure, respectively. Furthermore $\mathbf{x} = (x, y)$ represents the coordinate vector and $t$ is time.

The dependent variables are scaled using following set of characteristic values

$$\varphi_0 = \frac{RT}{F}, q_0 = 2c_0F, v_0 = \frac{D}{L}, p_0 = \frac{\eta_0 v_0}{L}$$

The characteristic concentration is related to the system size via the electric double layer thickness $\lambda_D$ by

$$\lambda_D = \left(\frac{\varepsilon RT}{2c_0F^2}\right)^{\frac{1}{2}}.$$

The spatial coordinates are scaled by the periodic segment length $L$ and time is scaled by the mixed relaxation time

$$t_0 = \frac{\lambda_D L}{D},$$

which represents a product of the Debye time (the diffusion time for the electric double layer) and the bulk relaxation time.

The dimensionless mathematical model describing situation in the electrolyte domain consists of the Poisson-Nernst-Planck equation, the Navier-Stokes equation and the equation of continuity [4].

$$\begin{gathered}
0 = -\tilde{\nabla}\cdot\left(\tilde{\nabla}\tilde{\varphi}\right) - \frac{\tilde{q}}{\tilde{\lambda}_D^2}, \\
\frac{1}{\tilde{\lambda}_D}\frac{\partial \tilde{c}}{\partial \tilde{t}} = -\tilde{\nabla}\cdot\tilde{\mathbf{J}}, \quad \tilde{\mathbf{J}} = \tilde{\mathbf{v}}\tilde{c} - \tilde{\nabla}\tilde{c} - \tilde{q}\tilde{\nabla}\tilde{\varphi}, \\
\frac{1}{\tilde{\lambda}_D}\frac{\partial \tilde{c}}{\partial \tilde{t}} = -\tilde{\nabla}\cdot\tilde{\mathbf{I}} - \frac{\tilde{q}}{\tilde{\lambda}_D^2}, \quad \tilde{\mathbf{I}} = \tilde{\mathbf{v}}\tilde{q} - \tilde{\nabla}\tilde{q} - \tilde{c}\tilde{\nabla}\tilde{\varphi}, \\
\frac{1}{\tilde{\lambda}_D}\frac{1}{\mathrm{Sc}}\frac{\partial \tilde{\mathbf{v}}}{\partial \tilde{t}} = -\tilde{\nabla}\cdot\left(\frac{\tilde{\mathbf{v}}\tilde{\mathbf{v}}}{\mathrm{Sc}} - \tilde{\nabla}\tilde{\mathbf{v}}\right) - \tilde{\nabla}\tilde{p} - \frac{\mathrm{Ra}}{\tilde{\lambda}_D^2}\tilde{q}\tilde{\nabla}\tilde{\varphi}, \\
0 = -\tilde{\nabla}\cdot\tilde{\mathbf{v}},
\end{gathered}$$

Tilde marks denote the dimensionless (scaled) variables. $\tilde{\mathbf{J}}$ and $\tilde{\mathbf{I}}$ represent the average ionic molar flux and the electric current density, respectively. Ra and Sc denote the Rayleigh and Schmidt numbers. Parameter $\tilde{\lambda}_D$ is the double layer thickness (the Debye length) scaled by the spatial period of the system (periodic segment length) $L$.

Situation in the electrode and dielectric domains can be described by the Laplace equation.

$$0 = -\tilde{\nabla}\cdot\left(\tilde{\nabla}\tilde{\varphi}\right)$$

The electric double layer consists of metal-side and electrolyte-side parts. The thickness of the electrolyte part is typically in the order of nanometers and thickness of the metal part is at least hundred times lower. In our model, the metal part of the double layer is represented by the surface electric charge density $\tilde{Q}$ defined only at the metal-electrolyte and metal-dielectric interfaces.

At the outer boundaries of the dielectric domains, the zero flux density is defined

$$0 = \mathbf{n}\cdot\left(\tilde{\nabla}\tilde{\varphi}\right).$$

At the outer electrode boundaries, the electric potential is defined as a function of time

$$\tilde{\varphi}(t) = \begin{cases} 1, & t \in [0\pi, \pi] \\ -1, & t \in [\pi, 2\pi] \end{cases}.$$

Four such signals shifted by 90 ° from each other are applied on the electrode arrays and form the traveling wave.

The left and right borders of the periodic segment are periodically coupled

$$\tilde{\xi}(0, \tilde{y}, \tilde{t}) \equiv \tilde{\xi}(1, \tilde{y}, \tilde{t}).$$

Here $\tilde{\xi}$ denotes the dimensionless dependent variables and their derivatives in the $x$-direction.

Definition of the electric charge density $\mathbf{I}$ is dependent on the subdomain material and hence on the mechanism of the charge transport. The total current density has two contributions, the Faradaic and the Maxwell currents. The Faradaic currents, $\mathbf{I}_\mathrm{F}$, rely on a presence of mobile charged particles. The Maxwell currents, $\mathbf{I}_\mathrm{M}$, can pass even through vacuum and they are generated changes of an electric field. The total electric current density is defined by

$$\tilde{\mathbf{I}}_\mathrm{tot} = \tilde{\mathbf{I}}_\mathrm{F} + \tilde{\mathbf{I}}_\mathrm{M}, \tilde{\mathbf{I}}_\mathrm{F} = \tilde{\mathbf{v}}\tilde{q} - \tilde{\nabla}\tilde{q} - \tilde{c}\tilde{\nabla}\tilde{\varphi}, \tilde{\mathbf{I}}_\mathrm{M} = -\tilde{\nabla}\tilde{V},$$

where $\tilde{V} = \partial_{\tilde{t}}\tilde{\varphi}$ is a derivative of the electric potential over time.

Propagation of the electric field across the electrode-dielectric interfaces is described by

$$\mathbf{n}\cdot\mathbf{I}_\mathrm{M}^{(d)} = -\mathbf{n}\cdot\mathbf{I}_\mathrm{F}^{(m)}.$$

Propagation of the electric field across the electrolyte-dielectric interfaces is given by

$$\mathbf{n}\cdot\mathbf{I}_\mathrm{M}^{(e)} = -\mathbf{n}\cdot\mathbf{I}_\mathrm{M}^{(d)}.$$

The superscripts $e$, $d$ and $m$ refer to the electrolyte, metal and dielectric domains, respectively.

Propagation of the electric field across the electrolyte-electrode interfaces is given by

$$\mathbf{n} \cdot \mathbf{I}_{\mathrm{M}}^{(e)} = -\mathbf{n} \cdot \mathbf{I}_{\mathrm{F}}^{(m)}.$$

The non-slip condition for velocity and non-permeability for mass transfer holds on all solid-electrolyte interfaces

$$\tilde{\mathbf{v}} = \mathbf{0},\ \tilde{\mathbf{J}}=\mathbf{0}$$

Value of the pressure is fixed in one arbitrary point of the electrolyte domain.

### 3. Use of COMSOL Multiphysics

The extension of the mathematical model introduced a rotation of vector field degenerated at the phase interfaces. A correct mathematical description is much convenient and accurate by the means of the COMSOL's weak form. The weak form is also able to handle the singularities occuring at the electrode corners.

The discontinuous driving is implemented as follows. At the beginning, the mesh and the geometry are assembled. Then, four versions of the boundary conditions are added and form four FEM structures. The FEM structures then undergo the mesh extension. Initial simulation starts from initial approximations. After one quarter of ac field period, the second FEM structure with changed periodical conditions uses the final system state as the initial approximation and simulation proceeds to the second quarter of the period. In this manner, the four FEM structures are used in a sequence to generate discontinuous traveling wave applied over the electrode array.

This stage-wise simulation also bypasses COMSOL's operational memory limitations and allows to perform simulations with longer timespan or with finer discretization in time.

Discretization of time has to be adjusted from isotropical to the exponential trend in order to capture the instantaneous changes in the electrode potential induce rapid and intense changes in the model quantities. It requires finer time-steps at the beginning and the end of the quarters of period.

### 4. Results & Discussion

The mathematical model allows studying the system behavior during transient.

To ensure, that the AC pump approaches the stable periodical regime (or is at least reasonably close), we take the $x$-component of velocity vector averaged over the computational domain, $u_{\mathrm{avg}}$, in a span of one period

$$u_{\mathrm{avg}}(T_i) = \frac{1}{LH}\int_D u(x,t)\,\mathrm{d}x\mathrm{d}y\,, t \in T_i,$$

where $T_i$ denotes the $i$-th period of the AC field.

Than we compare the averaged velocity during two consecutive periods. Integral of the squared difference is a measure of the system regime steadiness.

$$\delta u_{\mathrm{avg}} = \int_{T_i}\left[u_{\mathrm{avg}}(T_i) - u_{\mathrm{avg}}(T_{i-1})\right]^2 \mathrm{d}t.$$

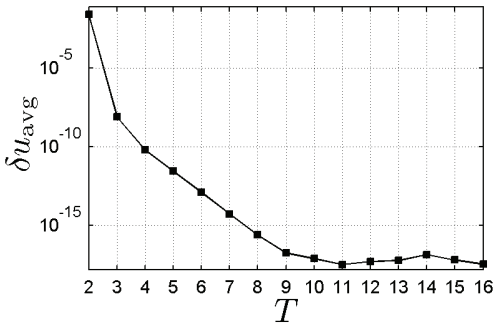


**Figure 2**. Transient stage. An integral of the squared differences between the averaged velocities over the period of AC field.

Each period after the transient consists of four quarters, which exhibit the same development of the averaged velocity. One quarter is depicted in Fig. 3.

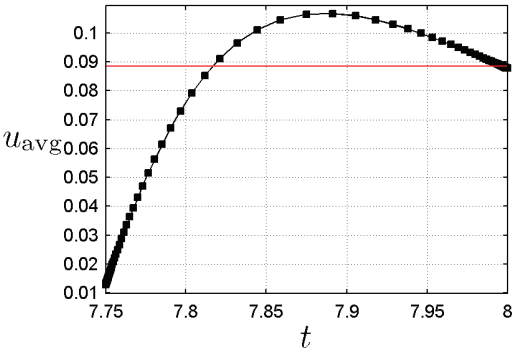


**Figure 3**. Development of the averaged stream-wise velocity over the last quarter of 8-th period of the AC signal.

The quarter starts with an accelerated phase caused by the switch in the driving field. An instantaneous change in the electrode polarity causes build-up of the electric potential above the electrodes. Bulges in the electric potential rise above one channel wall during one quarter and then appear above the opposite wall during the next quarter, see Fig. 4.

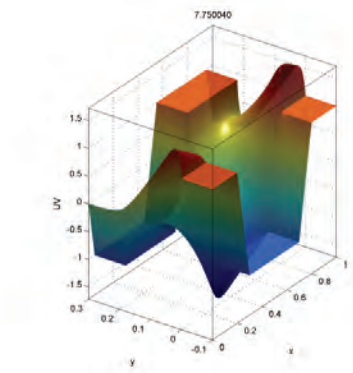


**Figure 4**. The electric potential distribution shortly after the signal switch. The flat areas represent the electrodes. There are noticeable bulges close to the electrodes on the bottom wall ($x = 0$).

The electroosmotic flow is enhanced since there is an additional potential drop (hence the driving force) in the stream-wise direction in the bulges. After the bulges disappear, see Fig. 5, the averaged velocity tends to exponentially fall to zero.

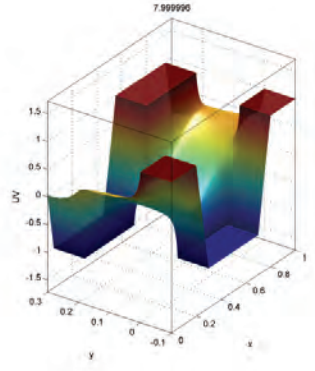


**Figure 5**. The steady electric potential distribution. The flat areas represent the electrodes.

The electric charge density also changes between the accelerated and the descending phase. The sign of the dominating charge above the electrodes changes as the averaged velocity approaches the maximum see Fig. 6.

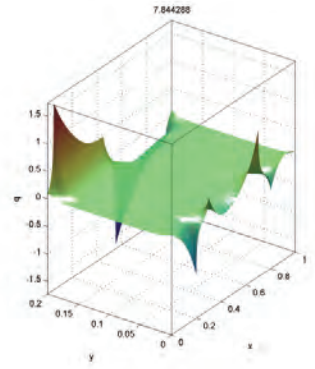


**Figure 6**. The electric charge density distribution during the averaged velocity maximum. The first and third electrode (cf. Fig. 1) are polarized in a bipolar manner.

Fig. 7 shows the flow patterns shortly after the ac field shift. This rather complicated flow develops into a steady structure (Fig. 8), which is disrupted by the next switch.

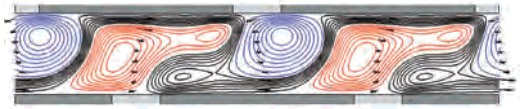

**Figure 7**. The flow patterns shortly after the AC field switch.

In the next quarter, the flow-structure is quite similar. The eddies are localized at the outlet corners of the

electrodes in the upper array and they rotate counter clock-wise.

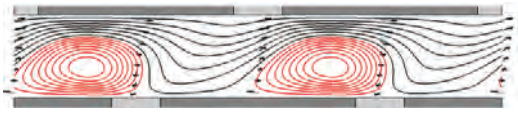

**Figure 8**. The steady flow patterns.

## 5. Conclusions

The existing mathematical model of an AC electroosmotic micropump has been extended by the additional domains and transformed into the weak form. The traveling-wave composed by continuous sinusoidal signals has been replaced by the set of discontinuous digital signals. The model solution procedure has been rearranged into a stage-wise sequence of simulations. The modeling domain was discretized anisotropically in both time and space in order to capture fast and localized dynamics occurring after the boundary conditions switches.

Our future work will be focused on optimization of the micropump performance and further development of the model. Finally, we plan to compare the results to experimental results as soon as will be fabricated in our laboratory.

## 6. References


1. A. Ramos et al, Ac electric-field-induced fluid flow on microelectrodes, *Journal of Colloid and Interface Science*, **217**, 420-422 (1999)
2. A. Ajdari, Pumping liquids using asymmetric electrode arrays, *Physical Review E*, **61**, R45-R48 (2000)
3. B.P. Cahill et al, Electro-osmotic streaming on application of traveling-wave electric field, *Physical Review E*, **70**, 036305 1-14 (2004)
4. J. Hrdlicka et al, Mathematical modeling of ac electroosmosis in microfluidic and nanofluidic chips using equilibrium and non-equilibrium approaches, *Journal of Applied Electrochemistry*, **40**, 967-980 (2009)


## 7. Acknowledgements


The authors thank for financial support to the grant of Czech Science Foundation 104/08/H055.